


Ultraviolet vision: photophysical properties of the unprotonated retinyl Schiff base in the Siberian hamster cone pigment

Andrea Bonvicini^{1,2} · Baptiste Demoulin¹ · Salvatore F. Altavilla² · Artur Nenov² ·
Mohsen M. T. El-Tahawy^{2,3} · Javier Segarra-Martí² · Angelo Giussani² ·
Victor S. Batista⁴ · Marco Garavelli^{1,2} · Ivan Rivalta¹ 

Received: 16 October 2015 / Accepted: 14 March 2016 / Published online: 2 April 2016
© Springer-Verlag Berlin Heidelberg 2016

Abstract The Siberian hamster ultraviolet (SHUV) visual pigment has an unprotonated Schiff-base (SB) retinyl chromophore in the dark state, which becomes protonated after photoexcitation during the early stages of the photobleaching cycle. While the photochemical relaxation processes of the SHUV remain poorly understood, they are expected to show significant differences when compared to those of the protonated SB (PSB) chromophore in visual rhodopsin. Here, we report a study of the photophysical properties of the SHUV unprotonated SB (SHUV-USB), based on multiconfigurational and multireference perturbative methods within a hybrid quantum mechanics/molecular mechanics scheme. Comparisons of multireference and time-dependent density functional theory results indicate that both methodologies predict an ionic excited state (S_1), similar to the PSB of rhodopsin, although its minimum has even bond-lengths in the central region of the retinyl polyene chain. The analysis of excited-state manifolds at the Franck–Condon region and S_1 minimum configuration

indicates that the skeletal relaxation initiated in the S_1 surface is likely to involve S_1/S_2 surface crossing. These results provide valuable insights for future studies of the SHUV-USB photoisomerization mechanism.

Keywords Retinal chromophores · UV pigment · Unprotonated Schiff base · Wavefunction methods · TD-DFT

1 Introduction

Visual perception is one of the most fascinating light-induced processes, initiated by the conversion of photons into conformational changes of photoreceptors. These visual pigments are G protein-coupled receptors (GPCR) of the retinylidene protein family that are embedded in the lipid membranes of specialized neurons, including cones and rods of the retina of vertebrates. Rhodopsin (Rh), the visual pigment of rod cells, is responsible for peripheral and night vision and remains one of the most widely studied photoreceptors. Light is absorbed by the 11-*cis*-retinyl chromophore (λ_{MAX} 498 nm), which is covalently bound to the Rh Lys296 amino acid residue by a protonated Schiff-base (PSB) linkage (Fig. 1) [1]. Light absorption triggers the retinyl 11-*cis* \rightarrow all-*trans* photoisomerization, which corresponds to the primary photochemical event in vertebrate vision.

Primitive nocturnal mammals have UV-sensitive ancestral pigments [2, 3], currently widespread in the animal kingdom. Fundamental studies of vertebrate UV pigments are, therefore, particularly important for understanding the evolution of photoreceptors [4]. A distinct aspect of UV-sensitive pigments, when compared to visual rhodopsin, is that the chromophore is bound to the protein by an

Published as part of the special collection of articles “Health & Energy from the Sun.”

✉ Ivan Rivalta
ivan.rivalta@ens-lyon.fr

Marco Garavelli
marco.garavelli@ens-lyon.fr

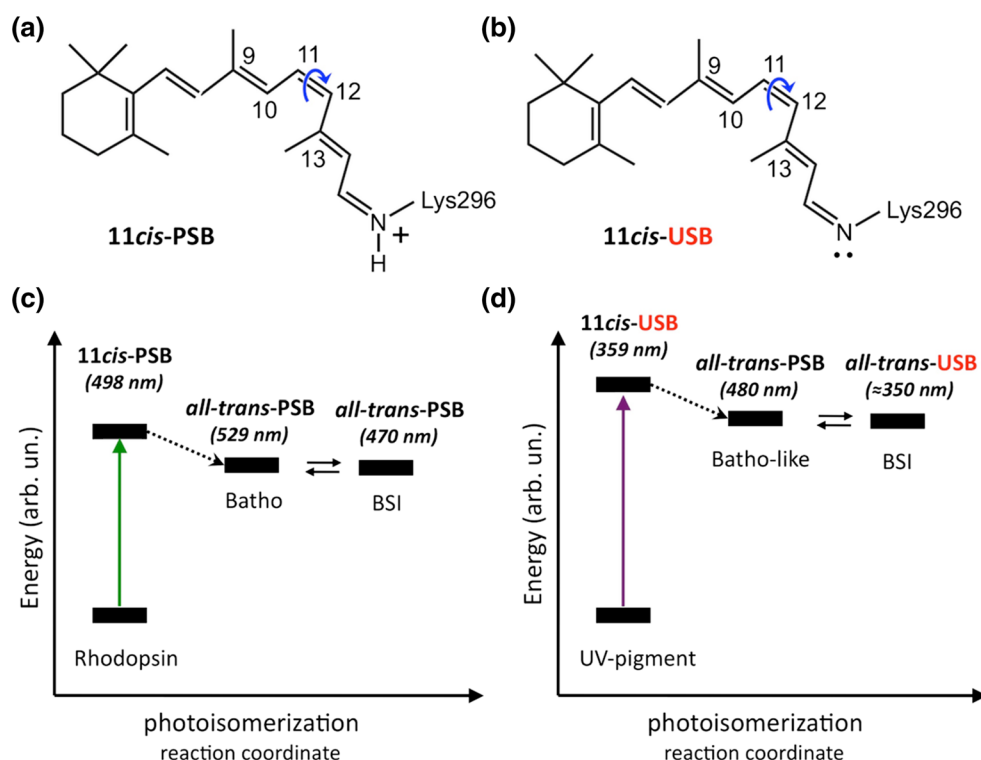
¹ Ens de Lyon, CNRS, Université Lyon 1, Laboratoire de Chimie UMR 5182, 69342 Lyon, France

² Dipartimento di Chimica “G. Ciamician”, Università di Bologna, V. F. Selmi 2, 40126 Bologna, Italy

³ Chemistry Department, Faculty of Science, Damanhour University, Damanhūr 22511, Egypt

⁴ Department of Chemistry, Yale University, New Haven, CT 06520-8107, USA

Fig. 1 Schematic representation of the 11-*cis* protonated (PSB) and unprotonated (USB) Schiff bases found in the dark state of rhodopsin (a) and Siberian hamster UV pigment (b). Early photointermediates experimentally detected in rhodopsin (c) and UV pigment (d) showing the preservation of the PSB in rhodopsin and the multiple changes of the protonation state in the UV pigment. The photorhodopsin intermediate in rhodopsin is omitted for clarity. Absorption λ_{MAX} reported in parentheses are taken from Refs. [6, 11]



unprotonated Schiff-base (USB) linkage in the dark state [5, 6]. Elucidating the fundamental interactions responsible for regulating the protonation state of the retinyl chromophore in UV pigments and the underlying dynamics triggered by UV photoexcitation is critical for understanding the photophysics of these ancestral pigments as well as for the design of biomimetic UV photochromic switches [7–10].

A comprehensive time-resolved study has been recently reported for the Siberian hamster (*Phodopus sungorus*) UV cone pigment [6], suggesting that the photoactivation mechanism involves multiple changes in the protonation state of the Schiff-base (SB) linkage (Fig. 1). The dark-adapted state is deprotonated. Upon photoexcitation, it generates an all-*trans* protonated intermediate, analogous to the bathorhodopsin intermediate of Rh, with spectroscopic fingerprints detected 300 ns after photoexcitation. The resulting protonated batho-like intermediate of the SHUV pigment equilibrates very quickly, in a timescale shorter than the spectral resolution of the experiment (ca. 7 ns) and of that observed in rhodopsin (ca. 40 ns), with a deprotonated blue-shifted intermediate (BSI). This observation implies the frequent occurrence of proton-transfer events in the early stages of the SHUV phototransduction mechanism, delineating a different scenario from rhodopsins (see Fig. 1c, d). In bovine Rh, in fact, the PSB is preserved up to the meta II state, i.e., up to large conformational changes of the transmembrane protein helices that transmit the signal to the cytoplasmatic surface [11].

Mutagenesis studies and computational structural models of the SHUV pigment have also been reported recently [5], suggesting that an extended network of hydrogen bonds regulates the protonation states of the SHUV by an inter-helical lock mechanism. The presence of a dark-state USB absorbing in the UV, the capability/propensity to change protonation states and the inter-helices interaction mechanisms are features that clearly differentiate the UV cone pigment from rhodopsins, potentially suggesting a new paradigm of opsins phototransduction. While different from Rh-PSB, the SHUV-USB features experimentally observed are not very surprising for chromophoric systems such as retinals, with high spectral sensitivity and tunable photophysical properties [12]. Since these properties are generally controlled by electrostatics and other environmental factors, theoretical studies aimed at their understanding have to account explicitly for the surroundings. Here, we report a hybrid quantum-mechanics (QM)/molecular mechanics (MM) study of the SHUV-USB photophysical properties to elucidate the photophysical properties of the SHUV as compared to those of rhodopsin. The QM/MM approach adopted is based on the multiconfigurational complete active space self-consistent field (CASSCF) method [13] together with its second-order perturbation theory extension (PT2) [14]. This methodology and the less computationally expensive time-dependent (TD) density functional theory (DFT) method have been extensively applied to retinal chromophores and rhodopsins [15, 16]. For comparison, we report calculations at the TD-DFT level with

CAM-B3LYP formalism [17, 18]. In particular, we focused on the singlet excited-state manifold in the Franck–Condon region and in the spectroscopic excited-state minimum, which has been characterized taking into account the occurrence of ultrafast proton-transfer processes. Our work aims to elucidate these photophysical properties to gain fundamental insights on UV visual perception.

2 Computational details

Our SHUV structural models are based on the DFT-QM/MM optimized structure [5], obtained by homology modeling based on the bovine rhodopsin crystal structure resolved at 2.2 Å [1]. We use the Rh structure residue numbering to facilitate the comparison between the two photoreceptors, although the SHUV-pigment primary sequence has a 5-residue shift in the N terminus (i.e., rhodopsin residue numbers are 5 greater than those of SHUV). We implemented a QM/MM two-layer scheme that allows for a combination of QM methods from different software packages [19]. The QM region involves the Glu113 counterion and the full retinal chromophore, which is linked to the rest of the protein, treated at the MM level with the Amber99ffSB [20] force field, by a hydrogen atom link [21] located at the N-C_ε(Lys296) bond. Multiconfigurational wavefunctions were built using the state-average (SA)-CASSCF methodology, as implemented in the Molcas 8.1 code [22], including 5, 7 or 10 states in the state-averaging procedure (i.e., SA5, SA7 and SA10). The relatively large state averages chosen are due to the fact that the spectroscopic state is not found among first five roots at the CASSCF levels and its root number is geometry dependent. SA-CASSCF calculations were followed by single-state (SS)-CASPT2 calculations to account for dynamic correlation, employing the commonly used CASPT2/CASSCF protocol. Hereafter, we refer to SA10 calculations as SA-CASSCF, or simply CASSCF, while the use of smaller SA is specified in the text. The ionization-potential-electron-affinity (IPEA) shift [25] was set to 0.0 a.u., and an imaginary shift of 0.2 a.u. was used throughout [26]. Oscillator strengths (*f*) were calculated making use of the complete/restricted active space state interaction method (CASSI/RASSI) [27, 28] employing the obtained CASSCF wavefunctions and CASPT2 energies. The Cholesky decomposition approach [29] was used to speed up the computations [30]. The CASSCF active space includes the entire π system of the chromophore, i.e., CAS(12,12), except for the calculations of the $n\pi^*$ states, where a CAS(14,13) was used.

Configuration interaction singles (CIS) [31] calculations were performed with the Gaussian 09 software [32], as the TD-DFT calculations, for which we employed the CAM-B3LYP exchange–correlation functional [17]. Mulliken

charges have been considered for estimating the charge-transfer differences between the ground state (GS) and the spectroscopic S_1 state.

For all calculations, the 6-31G* basis set was used. CASPT2/CASSCF and TD-DFT vertical excitations were compared with the DFT-QM/MM results based on the spectroscopy-oriented configuration interaction (SORCI + Q) method, as previously reported [5].

3 Results and discussion

The photophysical properties of the 11*cis*-USB of the Siberian hamster cone pigment are investigated using CASPT2/CASSCF and TD-DFT(CAM-B3LYP) methodologies within a hybrid QM/MM scheme. In the first section, the vertical excitation energies from the GS (S_0) to the first (S_1) and higher excited states in the singlet excited-state manifold have been calculated, along with their associated oscillator strengths (*f*). The nature of the bright spectroscopic state of the SHUV-pigment USB is compared with the ionic S_1 state of PSB in rhodopsin. The electronic transitions associated with the covalent S_2 and $n\pi^*$ states are also characterized in the Franck–Condon region to evaluate the potential role of these states in the USB photophysics. In the second section, the characterization of the spectroscopic excited-state minimum is performed at different levels of theory and compared with the structure of the rhodopsin PSB S_1 minimum. The energetics related to the protonation states of the SB in the ground- and excited-state minima in the SHUV pigment is then reported in the third section. Finally, the energy level variations in the singlet excited-state manifold upon relaxation along the spectroscopic state's potential energy surface are analyzed in the last section. Here, the nomenclature of the S_N states follows that initially defined in the FC region, even if surface crossings occur.

3.1 Franck–Condon region

The experimental UV–Vis spectrum of the SHUV pigment shows absorption maximum at λ_{MAX} equals to 359 nm (i.e., 3.45 eV) [6]. Theoretical prediction of the absorption maximum based on a homology model (from the bovine rhodopsin X-ray structure [1]) and multireference DFT-QM/MM (i.e., SORCI + Q/B3LYP/6-31G(d):Amber96) calculations are red-shifted by only 0.09 eV from the experimental value [5]. Using the previously reported homology model of the protein-embedded USB chromophore, we have evaluated the performances of other QM approaches widely employed in the photophysical and photochemical studies of retinal chromophores [15, 18], such as the TD-DFT(CAM-B3LYP/6-31G*) and the multireference

Table 1 Absorption maximum (λ_{MAX} in nm and excitation energies in eV) and the corresponding oscillator strengths (f) obtained at different levels of theory

Method	λ_{MAX} (nm)	Excitation energy (eV)	Osc. str. (f)
CAM-B3LYP	345	3.59	1.60
CASPT2/CASSCF	340	3.65	0.97
MS-CASPT2	389	3.19	0.92
SORCI + Q ^b	369	3.36	1.62
Exp. ^a	359	3.45	

The experimental and theoretical (SORCI + Q) data are taken from Refs. ^a [6], ^b [5]

CASPT2/CASSCF(12,12)/6-31G* methods within a QM/MM(Amber99) scheme [19], as described in Sect. 2. Table 1 shows the absorption maximum calculated at different levels of theory and the predicted oscillator strength of the bright S_1 state in the FC region. Both CAM-B3LYP and CASPT2/CASSCF results are blue-shifted by <0.2 eV (i.e., 3.59 and 3.65 eV, respectively) with respect to the experimental absorption maximum, a deviation that is within the expected error for these techniques. The use of a multistate MS-CASPT2 treatment has been found to give more reliable (and red-shifted) transition energies than SS-CASPT2 in rhodopsin when the QM model includes both the PSB and the negatively charged Glu113 counterion [12], a case in which the ionic S_1 and covalent S_2 states are found to be degenerated. In the QM region of our model the Glu113 counterion (Glu108 in the original SHUV-pigment sequence) is included but in its protonated form. In such a case, the S_1/S_2 degeneracy is not occurring, and as shown in Table 1, the MS-CASPT2 transition energy is red-shifted by 0.36 eV with respect to the SS-CASPT2

one, being 0.26 eV lower than the experimental value. The off-diagonal elements of the multistate PT2 Hamiltonian are found to be an order of magnitude larger than the upper limit (0.002 a.u.), indicating that the MS-CASPT2 treatment is not recommended in this case and it will not be considered further in this work [33].

The absorption maximum of the USB is referred to the $GS \rightarrow S_1$ transition, a bright electronic excitation with oscillation strength calculated to be 1.62 at the SORCI + Q level of theory. Similar oscillator strengths are found at both TD-DFT and CASPT2/CASSCF levels, being 1.60 and 0.97, respectively. This bright transition is associated with a $\pi\pi^*$ one-electron excitation from the highest occupied molecular orbital (HOMO, H) to the lowest unoccupied molecular orbital (LUMO, L), as for the spectroscopic state of rhodopsin PSB. Figure 2 shows these frontier orbitals, along with the molecular orbital involving the N lone pair (n) of the unprotonated SB, as calculated at the CASSCF(14,13) and CAM-B3LYP levels of theory. The $H \rightarrow L$ electron excitation in the USB of SHUV is associated with a small charge separation from the SB side (N-side) to the β -ionone ring side (β -side). By defining the separation of these two sides at the central $C_{11}=C_{12}$ double bond, CASSCF and TD-DFT calculations indicate a transfer of a 0.2 and 0.13, respectively, positive charge from the N- to the β -side associated with an increase of the permanent dipole moment of the USB by ca. 5.5 and 6.2 Debye, respectively. Therefore, the spectroscopic state of the USB has an ionic character with an intramolecular charge transfer (CT) that is much less pronounced than what observed in the PSB of rhodopsin, where 52 % of the PSB positive charge is transferred to the β -side upon vertical excitation [12] and the permanent dipole moment difference is ca. 15 Debye [34, 35]. These

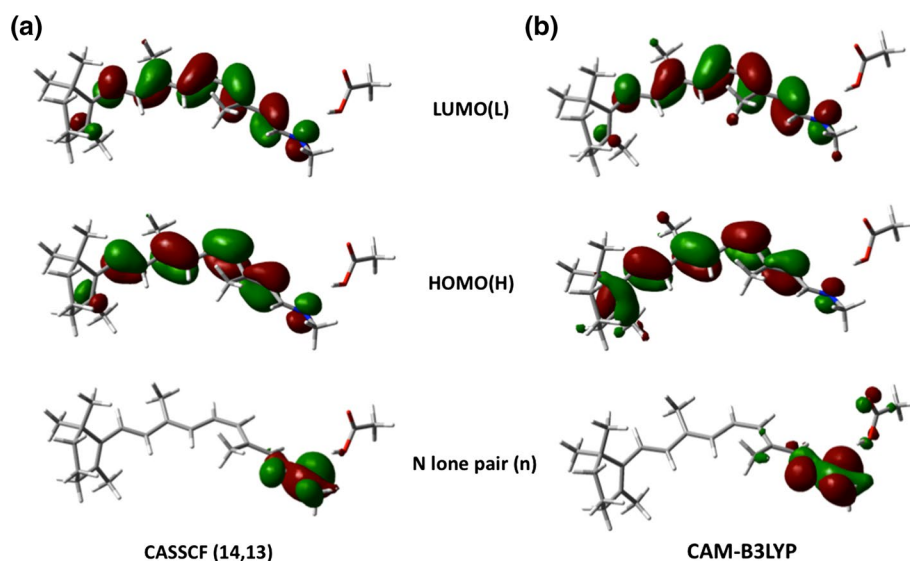
Fig. 2 Frontier orbitals of the unprotonated Schiff base in the SHUV pigment, including the N lone pair (n), calculated at the CASSCF(14,13) and TD-DFT(CAM-B3LYP) levels of theory

Table 2 Vertical GS $\rightarrow S_N$ (with $1 \leq N \leq 3$) excitation energies (in eV) and the corresponding oscillator strengths in the unprotonated Schiff base of the SHUV pigment calculated at the CASPT2/CASSCF(6-31G*) and CAM-B3LYP(6-31G*) levels of theory

Excitation	Root #	Excitation energy (eV)	Osc. str. (<i>f</i>)
CASPT2/CASSCF			
H \rightarrow L	2	3.65 (2.50) ^a	0.97 (0.74) ^a
(H \Rightarrow L) ²	3	3.98 (3.56) ^a	0.00 (0.27) ^a
n \rightarrow L	4	4.40	0.01
TD-DFT			
H \rightarrow L	2	3.59	1.60
n \rightarrow L	3	4.78	0.12

A CASSCF(14,13) active space was used for transition energy calculation of the $n\pi^*$ ($n \rightarrow L$) state. SS-CASPT2/CASSCF(12,12) calculations are compared with previously reported data of the PSB in rhodopsin at MS-CASPT2/CASSCF(12,12) level, ^a Ref. [12]

results are in line with previous experimental and theoretical investigations on model systems [35, 36].

The frontiers and lone-pair orbitals depicted in Fig. 2 are those involved in the lowest three excited states of the USB. In fact, as shown in Table 2, the first three excited states obtained at the CASPT2/CASSCF level involve the H \rightarrow L one-electron excitation (i.e., the spectroscopic S_1 ionic state), the (H \Rightarrow L)² double excitation (i.e., the S_2 covalent state) and the n \rightarrow L one-electron excitation (i.e., the S_3 $n\pi^*$ state). In contrast to rhodopsin, the S_1 and S_2 states are relatively close to each other in the SHUV-USB, with a S_1/S_2 energy gap of 0.33 eV (vs 1.06 eV in Rh). The GS $\rightarrow S_2$ transition is found to be dark in the SHUV pigment, with exceedingly small associated oscillator strength, while the calculated oscillator strength of the GS $\rightarrow S_1$ transition is slightly higher in the SHUV-USB than in Rh-PSB.

In the singlet excited-state manifold of retinal Schiff bases, the main qualitative difference between an unprotonated and a protonated SB is due to the presence of $n\pi^*$ states that appear when the N atom of the SB linkage is deprotonated. The lowest $n\pi^*$ state in the SHUV pigment is calculated to be the third singlet excited state (S_3) at the CASPT2/CASSCF(14,13) level, corresponding to a dark n \rightarrow L electronic transition (with $f = 0.01$) lying at 4.40 eV from the GS. At the CAM-B3LYP level this transition energy is larger (4.78 eV) and slightly brighter ($f = 0.12$) with respect to the CASPT2/CASSCF results. The standard TD-DFT approach adopted in this work does not account for double singlet excitations; therefore, the (H \Rightarrow L)² double excitation is absent in the CAM-B3LYP singlet excited-state manifold and the $n\pi^*$ state is the closest singlet state to the spectroscopic S_1 state. While both covalent and $n\pi^*$ states are found to be dark and not degenerate with the S_1 state in the FC region, their role in the photophysics cannot be excluded based on the reported results. In the following

sections, we characterize the structure of the S_1 excited-state minimum and evaluate the changes in the singlet excited-state manifold of the SHUV-USB.

3.2 Excited-state minimum

The first photoinduced event in the photoisomerization path of the 11*cis*-PSB in rhodopsin is the skeletal relaxation of the retinal conjugated system. Upon excitation to the spectroscopic (S_1) excited state, the coherent wavepacket motion from the photoexcited Franck–Condon region involves a primary bond relaxation and a subsequent torsional motion along the central C₁₁–C₁₂ bond that gives access to the conical intersection seam, leading to the all-*trans* photoproduct [37]. The characterization of the minimum energy path (MEP) of the photoisomerization reaction of Rh-PSB has indicated the presence of a fully relaxed planar stationary point (energy minimum) [16]. Here, we have investigated the initial part of the photoisomerization MEP of the SHUV-USB by characterizing the S_1 excited-state minimum.

Figure 3a shows the differences between the ground (S_0) and excited (S_1) minima of the Rh-PSB and the SHUV-USB, as obtained by geometry optimization at the SA5-CASSCF(12,12) level. As expected, the GS geometries differ only by minimal bond-length changes in the terminal N–C₁₅ region, due to the different protonation states of the imine group in the two Schiff bases. The single-/double-bond alternation of the Rh-PSB ground-state geometry is almost completely inverted in its excited-state minimum. In contrast, the excited-state SHUV-USB minimum shows uniform bond-lengths along most of the retinal polyene chain. In particular, the sequence of ground-state single (C₈–C₉, C₁₀–C₁₁, C₁₂–C₁₃ and C₁₄–C₁₅) and double bonds (C₉–C₁₀, C₁₁–C₁₂, C₁₂–C₁₃) that show the largest bond inversion in the excited-state minimum of Rh-PSB have even bond-lengths (i.e., around 1.40–1.41 Å) in the SHUV-USB excited-state minimum, a structural feature analogous to that of neutral polyenes.

In order to verify the consistency of the CASSCF geometry optimization, which indicates uniform bond-lengths in the excited-state minimum of the SHUV-USB, we have performed computations also at the CIS and TD-DFT levels of theory. Both the CIS(6-31G*) and the CAM-B3LYP(6-31G*) excited-state geometry optimizations provide a nearly identical S_1 minimum, as depicted in Fig. 3b. The two different S_1 minimum geometries found in Rh-PSB and SHUV-USB very closely remind the two different local minima recently characterized along the photoisomerization path of artificial rhodopsin mimics [38]. Two S_1 local minima structures with even bond-lengths (EBL) or alternate bond-lengths (ABL) in the central part of the PSB (called LE and CT structures, respectively) were proposed

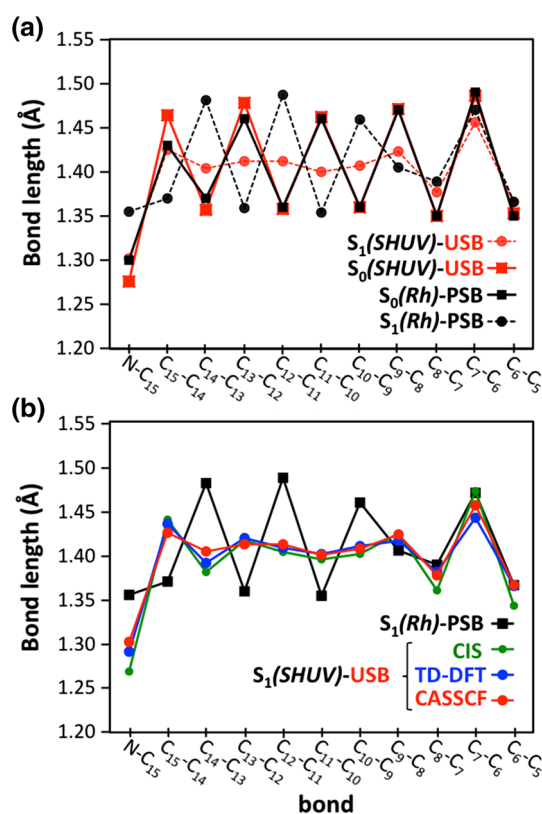


Fig. 3 **a** Bond-length alternation in the ground (S₀) and excited (S₁) minima of the PSB in rhodospin (Rh) and USB in UV pigment (SHUV) calculated at the CASSCF(12,12) level of theory. **b** Comparison of the S₁ excited-state minimum of the SHUV-USB calculated at different levels of theory, including the CIS, CAM-B3LYP (TD-DFT), and the CASSCF(12,12) methods and using the 6-31G* basis set

to explain the two fluorescence bands of the rhodopsin protein mimics. It is worth noting that, in contrast with the ABL structure, the EBL minimum of the PSB in the rhodopsin mimics could not be found by optimizing the spectroscopic state at the CASSCF level, and a CASPT2 energy profile has been constructed to determine the presence of two flat minima on the S₁ potential energy surface. These results indicate that the topology of the CASSCF potential energy surface, which does not account for dynamic electron correlation, could be significantly different from the more reliable CASPT2 surface [39]. For this reason, we have performed a rigid scan along a bond-length alternation (BLA) coordinate obtained by linear interpolation between the EBL and the ABL structures, as depicted in Fig. 4. The uphill energy profile derived at both the SA7-CASSCF and CASPT2/SA7-CASSCF levels, the latter representing an upper limit of the CASPT2 S₁ potential energy surface, indicates that the ABL structure is destabilized with respect to the EBL minimum obtained at the CASSCF level. These results suggest that the spectroscopic state can be trapped

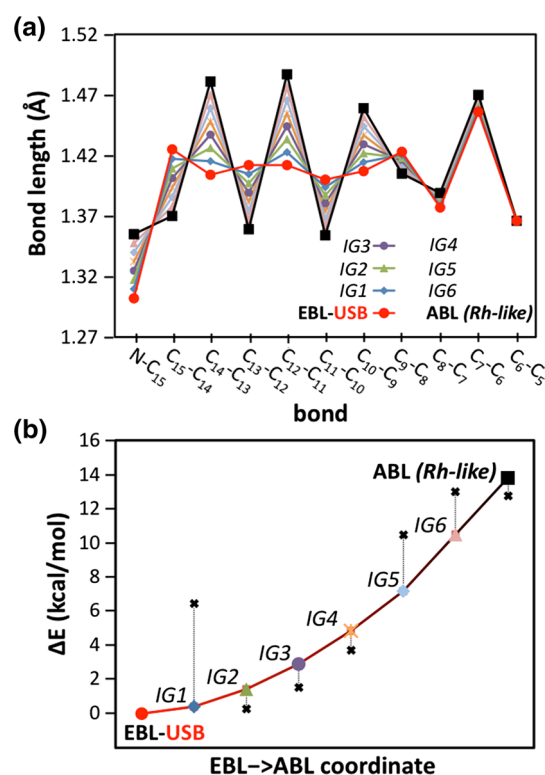


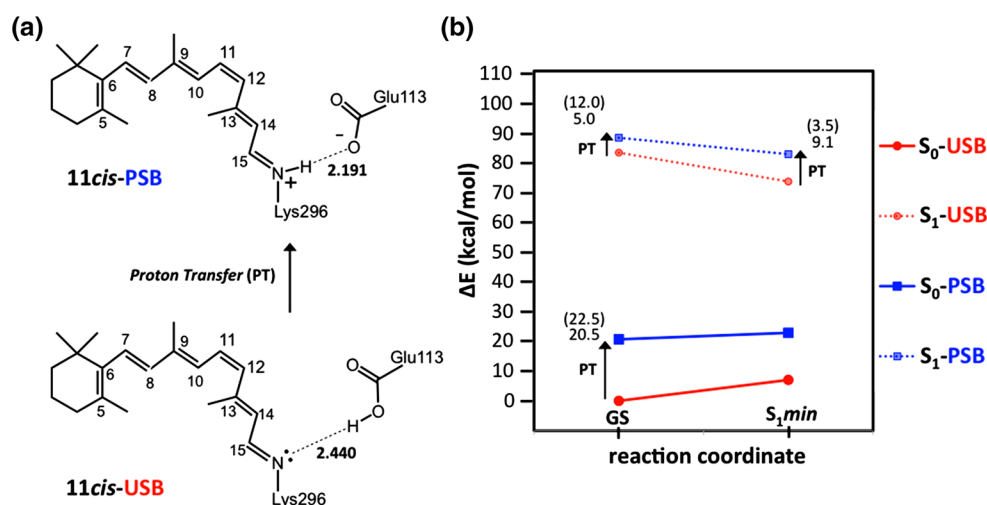
Fig. 4 Bond lengths in the SHUV-USB S₁(H → L) minimum having even bond-lengths (EBL), in the rhodopsin-like structure with alternate bond-lengths (ABL) and in the linearly interpolated geometries (IG1-6) along the EBL → ABL bond-length alternation pathway **(a)**. SA7-CASSCF (colored symbols) and CASPT2-corrected (black crosses) energy profile of the S₁(H → L) state along the EBL → ABL path **(b)**

in a local minimum with a relatively short (not elongated) C₁₁–C₁₂ bond that could slow down the photoisomerization process with respect to the Rh-PSB case, where the presence of an ABL minimum give rises to a barrierless clockwise rotation along the C₁₁–C₁₂ single bond. However, in order to achieve a more comprehensive picture of the photoisomerization pathway of the 11*cis*-USB in the SHUV pigment, an extended analysis of the excited-state manifold at the spectroscopic excited-state minimum and an assessment of possible changes in the SB protonation state are required.

3.3 Destabilization of a protonated Schiff base

Transient absorption measurements provided evidences of proton-transfer processes occurring during the early stage of the SHUV-USB photobleaching cycle [6]. In particular, the 11*cis*-SB is unprotonated in the dark state and gets protonated immediately after photoisomerization. The protonated photointermediate resembles the PSB bathorhodopsin intermediate of Rh (batho-like intermediate), and

Fig. 5 **a** Proton-transfer reaction in the SHUV pigment with residue numbering based on the Rh structure. **b** TD-DFT energy profile comparing the S_1 excited-state relaxation pathway of the SHUV-USB (in red) and SHUV-PSB (in blue) species. CASPT2/CASSCF results are reported in parentheses



it is in equilibrium with a blue-shifted intermediate (BSI) possessing a USB. The mixture of photointermediates with different protonation states equilibrates in a timescale (<10 ns) much faster than that of its formation (ca. 300 ns) and decay (few μ s) to subsequent intermediates [6]. These results suggest that the occurrence of proton transfers in the early stage of the photoisomerization process is more likely in the SHUV than in Rh, where all the photointermediates preserve a PSB until the meta II intermediate is formed, in the ms timescale. Unfortunately, the reported time-resolved electronic spectroscopy experiments do not have enough temporal resolution (only 7 ns) to resolve the absorption properties of photointermediates earlier than the batho-like, such as the photorhodopsin detected in Rh, and to exclude the occurrence of proton transfers at the very early stages of the photoisomerization process, i.e., in the fs–ps timescale.

The results reported in the previous section suggest a scenario in which the photoinduced process of the SHUV-pigment retinal chromophore is slowed down by the presence of an “inactive” excited-state minimum, i.e., an EBL minimum associated with a USB. This scenario contrasts with the common picture of the retinal isomerization of PSB in rhodopsin, which involves an ABL excited-state minimum and it occurs in an ultrafast timescale (ca. 200 fs). Since the reported time-resolved experiments do not provide information on the protonation states of the SHUV-USB in the ultrafast timescale, we have investigated the thermodynamics of the proton-transfer processes in the FC and spectroscopic excited-state minimum, as illustrated in Fig. 5.

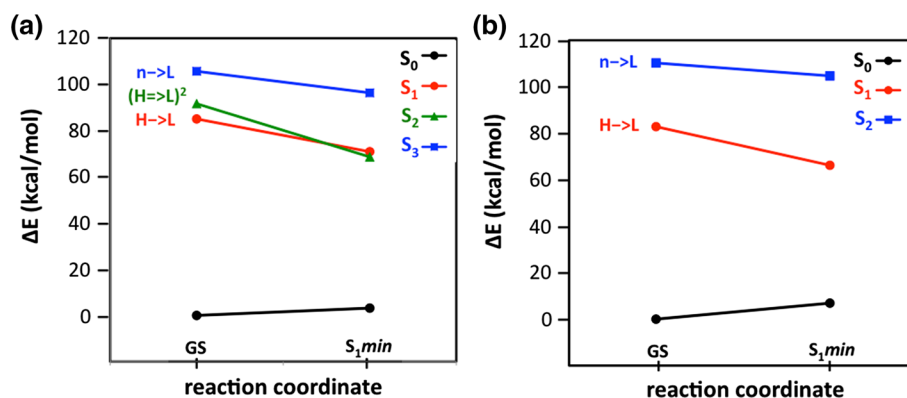
Figure 5b shows the comparison between the S_1 excited-state relaxation of the SHUV-USB and SHUV-PSB, calculated at both the CASPT2/CASSCF and CAM-B3LYP levels. The proton transfer from the Glu113 to the N atom of the USB in the UV-pigment ground state is associated with a total energy difference of +20.5 kcal/mol at the

CAM-B3LYP level (+22.5 kcal/mol at the CASPT2/CASSCF level), fully consistent with the experimental observation of a USB in the UV-pigment dark state [6]. The SHUV-PSB is predicted to absorb in the visible violet at 425 nm (67.2 kcal/mol) at the TD-DFT level and 388 nm (73.6 kcal/mol) at the CASPT2/CASSCF level. As a consequence, the PSB is found to be less stable than the USB also in the excited state at both TD-DFT and CASPT2/CASSCF levels, with an uphill proton-transfer process requiring 5.0 and 12.0 kcal/mol, respectively. As in the FC region, the USB is calculated to be more stable than the PSB at the geometry of the S_1 excited-state minimum, with a total energy difference of 9.1 and 3.5 kcal/mol at the TD-DFT and CASPT2/CASSCF levels, respectively. Notably, the SHUV-PSB minimum of the excited state is an ABL minimum analogous to the Rh-PSB one. These results suggest that the USB is very stable in the ground state of the SHUV pigment, in agreement with experiments, and that the photoinduced proton transfer is unlikely to happen on the S_1 excited-state surface since at both FC and S_1 geometries the USB is energetically favored with respect to the PSB.

3.4 Singlet excited-state manifolds

As mentioned in the previous sections, the PSB isomerization in rhodopsin involves wave-packet motion on a single potential energy surface, the spectroscopic S_1 excited state surface. However, other photochemical mechanisms exist and could be considered for the photoisomerization of the SHUV-USB, including (allowed or avoided) surface crossing among singlet excited-state surfaces or inter-system crossing between surfaces with different spin multiplicities. These alternative photochemical mechanisms would slow down the SHUV-USB *cis-trans* photoisomerization, for which there is a lack of experimental

Fig. 6 Evolution of energy levels of the singlet (S_N) excited states of the SHUV-USB along the S_1 relaxation pathway calculated at both CASPT2/CASSCF (a) and CAM-B3LYP (b) levels of theory



information regarding the reaction timescale. Therefore, the presence of excited-state surface crossings could not be excluded a priori in the early stage of the USB photoisomerization. For this reason, we have characterized the singlet excited-state manifold of the SHUV-USB in both the ground- and S_1 excited-state minima.

Figure 6 shows the positions of the S_2 and S_3 excited states along the potential energy profile of the S_1 excited-state relaxation pathway of the SHUV-USB calculated at both CASPT2/SA5-CASSCF (Fig. 6a) and CAM-B3LYP (Fig. 6b) levels of theory. As described in Sect. 3.2, the lowest three excited states of the USB in the FC region are the spectroscopic S_1 ionic state, the S_2 covalent state involving a $(H \Rightarrow L)^2$ double excitation and the S_3 $n\pi^*$ state. At the structure of the S_1 minimum, CASPT2/SA5-CASSCF calculations indicate that the S_2 excited state lies below the spectroscopic state minimum while the S_3 $n\pi^*$ state energy level is unaffected. Therefore, while the $n\pi^*$ state is almost unperturbed by the skeletal deformations along the S_1 relaxation pathway, the $(H \Rightarrow L)^2$ double excitation is highly stabilized and a S_1/S_2 surface crossing could occur prior reaching the EBL S_1 minimum. It is worth mentioning that CASSCF energy profiles significantly differ from the CASPT2/CASSCF ones, with all excited states significantly destabilized with respect to the GS minimum when the dynamic correlation is not accounted for. In particular, at CASSCF level the covalent S_2 and $n\pi^*$ states are found at 11–15 kcal/mol higher energies with respect to CASPT2/CASSCF profiles at both FC and S_1 minimum geometries, while the destabilization of the ionic S_1 state is significantly larger, being +55 and +63 kcal/mol at the FC and the S_1 minimum geometries, respectively. These results indicate strong differential correlation effects that certainly reduce the accuracy of the CASPT2/CASSCF results. Nevertheless, it has been previously shown that, even when strong differential correlation effects take place, the CASPT2/CASSCF protocol is capable of yielding a qualitatively right picture of the energetic profiles [40]. More rigorous investigations require computations of CASPT2 gradients, and

future work will focus on the quantitative effects of employing CASPT2 gradients by using novel approaches [39].

The outcome opens to a scenario where an “active” ABL structure can be reached on the S_2 on the potential energy surface, its investigation being currently in progress. Notably, the CAM-B3LYP results match the CASPT2/CASSCF energy trend of the S_3 $n\pi^*$ state, but the $(H \Rightarrow L)^2$ double excitation cannot be described using such standard TD-DFT approach. Thus, considering the role that the S_2 state could play on the SHUV-USB photoisomerization we conclude that a methodology that accounts for double excitations is mandatory for an appropriate study of the photoisomerization pathway of the SHUV pigment. Finally, the occurrence of singlet/triplet inter-system crossings cannot be excluded a priori and future investigations in this direction would provide other important pieces of information for the elucidation of the USB photoisomerization in the SHUV pigment.

4 Concluding remarks

We have investigated the basic photophysical properties of the Siberian hamster ultraviolet (SHUV) visual pigment, containing an UV-active unprotonated retinal Schiff base (SHUV-USB) chromophore, using multiconfigurational and multireference perturbative methods within a hybrid QM/MM scheme based on a previously reported homology model of the pigment. Multireference calculations have been compared with time-dependent density functional theory results, showing good agreement in the description of the ionic nature of the (S_1) excited state, analogous to the rhodopsin PSB. The excited-state minimum energy configuration exhibits a weak bond-length alternation in the central region of the retinal polyene chain, in contrast with rhodopsin where the minimum energy photoisomerization path involves an alternate bond-length minimum with a central “active” C_{11} – C_{12} single bond. We have also analyzed the singlet excited-state manifolds in both the Franck–Condon

region and the S_1 minimum. Our results suggest the presence of a S_1/S_2 excited-state surface crossing during the skeletal relaxation on the S_1 potential energy surface, indicating involvement of the covalent S_2 state in the SHUV-USB photochemistry. These results provide the basis for further studies of the SHUV-USB photoisomerization mechanism, which requires an appropriate description of the two-electron excitation associated with the covalent S_2 state.

Acknowledgments V.S.B. acknowledges supercomputer time from NERSC and the Yale High Performance Computing Center, and support from NSF Grant CHE-1465108. MG acknowledges support by the European Research Council Advanced Grant STRATUS (ERC-2011-AdG No. 291198). IR gratefully acknowledges the support of the École Normale Supérieure de Lyon (Fonds Recherche 900/S81/BS81-FR14). We acknowledge the use of HPC resources of the “Pôle Scientifique de Modélisation Numérique” at the ENS-Lyon, France.

References

- Okada T, Sugihara M, Bondar AN, Elstner M, Entel P, Buss V (2004) The retinal conformation and its environment in rhodopsin in light of a new 2.2 angstrom crystal structure. *J Mol Biol* 342(2):571–583
- Bowmaker JK (1998) Evolution of colour vision in vertebrates. *Eye* 12:541–547
- Hunt DM, Wilkie SE, Bowmaker JK, Poopalasundaram S (2001) Vision in the ultraviolet. *Cell Mol Life Sci* 58(11):1583–1598
- Mooney V, Sekharan S, Liu J, Guo Y, Batista VS, Yan ECY (2015) Kinetics of thermal activation of an ultraviolet cone pigment. *J Am Chem Soc* 137(1):307–313
- Sekharan S, Mooney VL, Rivalta I, Kazmi MA, Neitz M, Neitz J, Sakmar TP, Yan ECY, Batista VS (2013) Spectral tuning of ultraviolet cone pigments: an interhelical lock mechanism. *J Am Chem Soc* 135(51):19064–19067
- Mooney VL, Szundi I, Lewis JW, Yan ECY, Kliger DS (2012) Schiff base protonation changes in Siberian hamster ultraviolet cone pigment photointermediates. *Biochemistry* 51(12):2630–2637
- Birge RR (1990) Photophysics and molecular electronic applications of the rhodopsins. *Annu Rev Phys Chem* 41:683–733
- Briand J, Bram O, Rehault J, Leonard J, Cannizzo A, Chergui M, Zanirato V, Olivucci M, Helbing J, Haacke S (2010) Coherent ultrafast torsional motion and isomerization of a biomimetic dipolar photoswitch. *Phys Chem Chem Phys* 12(13):3178–3187
- Lumento F, Zanirato V, Fusi S, Busi E, Latterini L, Elisei F, Sinicropi A, Andruniow T, Ferre N, Basosi R, Olivucci M (2007) Quantum chemical modeling and preparation of a biomimetic photochemical switch. *Angew Chem Int Ed* 46(3):414–420
- Sinicropi A, Martin E, Ryazantsev M, Helbing J, Briand J, Sharma D, Leonard J, Haacke S, Cannizzo A, Chergui M, Zanirato V, Fusi S, Santoro F, Basosi R, Ferre N, Olivucci M (2008) An artificial molecular switch that mimics the visual pigment and completes its photocycle in picoseconds. *Proc Natl Acad Sci USA* 105(46):17642–17647
- Ahuja S, Smith SO (2009) Multiple switches in G protein-coupled receptor activation. *Trends Pharmacol Sci* 30(9):494–502
- Tomasello G, Olaso-Gonzalez G, Altoe P, Stenta M, Serrano-Andres L, Merchan M, Orlandi G, Bottoni A, Garavelli M (2009) Electrostatic control of the photoisomerization efficiency and optical properties in visual pigments: on the role of counterion quenching. *J Am Chem Soc* 131(14):5172–5186
- Roos BO (1987) Ab initio methods in quantum chemistry: part II. Wiley, Chichester
- Andersson K, Malmqvist PA, Roos BO (1992) 2nd-order perturbation-theory with a complete active space self-consistent field reference function. *J Chem Phys* 96(2):1218–1226
- Huix-Rotllant M, Filatov M, Gozem S, Schapiro I, Olivucci M, Ferre N (2013) Assessment of density functional theory for describing the correlation effects on the ground and excited state potential energy surfaces of a retinal chromophore model. *J Chem Theory Comput* 9(9):3917–3932
- Rivalta I, Nenov A, Garavelli M (2014) Modelling retinal chromophores photoisomerization: from minimal models in vacuo to ultimate bidimensional spectroscopy in rhodopsins. *Phys Chem Chem Phys*. doi:10.1039/c4cp55211j
- Yanai T, Tew DP, Handy NC (2004) A new hybrid exchange-correlation functional using the Coulomb-attenuating method (CAM-B3LYP). *Chem Phys Lett* 393(1–3):51–57
- Rostov IV, Amos RD, Kobayashi R, Scalmani G, Frisch MJ (2010) Studies of the ground and excited-state surfaces of the retinal chromophore using CAM-B3LYP. *J Phys Chem B* 114(16):5547–5555
- Altoe P, Stenta M, Bottoni A, Garavelli M (2007) A tunable QM/MM approach to chemical reactivity, structure and physico-chemical properties prediction. *Theor Chem Acc* 118(1):219–240
- Hornak V, Abel R, Okur A, Strockbine B, Roitberg A, Simmerling C (2006) Comparison of multiple amber force fields and development of improved protein backbone parameters. *Proteins: Struct Funct Bioinform* 65(3):712–725
- Senn HM, Thiel W (2009) QM/MM methods for biomolecular systems. *Angew Chem Int Ed* 48(7):1198–1229
- Aquilante F, Autschbach J, Carlson R, Chibotaru L, Delcey MG, De Vico L, Fernández Galván I, Ferré N, Frutos LM, Gagliardi L, Garavelli M, Giussani A, Hoyer C, Li Manni G, Lischka H, Ma D, Malmqvist PA, Müller T, Nenov A, Olivucci M, Pedersen TB, Peng D, Plasser F, Pritchard B, Reiher M, Rivalta I, Schapiro I, Segarra-Martí J, Stenrup M, Truhlar DG, Ungur L, Valentini A, Vancoillie S, Veryazov V, Vysotskiy V, Weingart O, Zapata F, Lindh R (2016) Molcas 8: new capabilities for multiconfigurational quantum chemical calculations across the periodic table. *J Comput Chem* 37(5):506–541
- Karlstrom G, Lindh R, Malmqvist PA, Roos BO, Ryde U, Veryazov V, Widmark PO, Cossi M, Schimmelpfennig B, Neogrady P, Seijo L (2003) MOLCAS: a program package for computational chemistry. *Comput Mater Sci* 28(2):222–239
- Aquilante F, De Vico L, Ferre N, Ghigo G, Malmqvist PA, Neogrady P, Pedersen TB, Pitonak M, Reiher M, Roos BO, Serrano-Andres L, Urban M, Veryazov V, Lindh R (2010) Software news and update MOLCAS 7: the next generation. *J Comput Chem* 31(1):224–247
- Ghigo G, Roos BO, Malmqvist PA (2004) A modified definition of the zeroth-order Hamiltonian in multiconfigurational perturbation theory (CASPT2). *Chem Phys Lett* 396(1–3):142–149
- Forsberg N, Malmqvist PA (1997) Multiconfiguration perturbation theory with imaginary level shift. *Chem Phys Lett* 274(1–3):196–204
- Malmqvist PA, Roos BO (1989) The Casscf state interaction method. *Chem Phys Lett* 155(2):189–194
- Malmqvist PA, Roos BO, Schimmelpfennig B (2002) The restricted active space (RAS) state interaction approach with spin-orbit coupling. *Chem Phys Lett* 357(3–4):230–240
- Aquilante F, Lindh R, Pedersen TB (2007) Unbiased auxiliary basis sets for accurate two-electron integral approximations. *J Chem Phys* 127(11):114107
- Aquilante F, Malmqvist PA, Pedersen TB, Ghosh A, Roos BO (2008) Cholesky decomposition-based multiconfiguration second-order perturbation theory (CD-CASPT2): application to the

- spin-state energetics of Co-III(diiminato)(NPh). *J Chem Theory Comput* 4(5):694–702
31. Foresman JB, Headgordon M, Pople JA, Frisch MJ (1992) Toward a systematic molecular-orbital theory for excited-states. *J Phys Chem* 96(1):135–149
 32. Frisch MJ, Trucks GW, Schlegel HB, Scuseria GE, Robb MA, Cheeseman JR, Scalmani G, Barone V, Mennucci B, Petersson GA, Nakatsuji H, Caricato M, Li X, Hratchian HP, Izmaylov AF, Bloino J, Zheng G, Sonnenberg JL, Hada M, Ehara M, Toyota K, Fukuda R, Hasegawa J, Ishida M, Nakajima T, Honda Y, Kitao O, Nakai H, Vreven T, Montgomery JA Jr, Peralta JE, Ogliaro F, Bearpark M, Heyd JJ, Brothers E, Kudin KN, Staroverov VN, Kobayashi R, Normand J, Raghavachari K, Rendell A, Burant JC, Iyengar SS, Tomasi J, Cossi M, Rega N, Millam JM, Klene M, Knox JE, Cross JB, Bakken V, Adamo C, Jaramillo J, Gomperts R, Stratmann RE, Yazyev O, Austin AJ, Cammi R, Pomelli C, Ochterski JW, Martin RL, Morokuma K, Zakrzewski VG, Voth GA, Salvador P, Dannenberg JJ, Dapprich S, Daniels AD, Farkas Ö, Foresman JB, Ortiz JV, Cioslowski J, Fox DJ (2009) Gaussian 09, Revision A.1. Gaussian, Inc., Wallingford, CT
 33. Serrano-Andres L, Merchan M, Lindh R (2005) Computation of conical intersections by using perturbation techniques. *J Chem Phys* 122(10):104107
 34. Mathies RA (1999) Photons, femtoseconds and dipolar interactions: a molecular picture of the primary events in vision. *Novartis Found Symp* 224:70–84 **discussion 84–101**
 35. Mathies R, Stryer L (1976) Retinal has a highly dipolar vertically excited singlet-state: implications for vision. *Proc Natl Acad Sci USA* 73(7):2169–2173
 36. Hufen J, Sugihara M, Buss V (2004) How the counterion affects ground- and excited-state properties of the rhodopsin chromophore. *J Phys Chem B* 108(52):20419–20426
 37. Polli D, Altoe P, Weingart O, Spillane KM, Manzoni C, Brida D, Tomasello G, Orlandi G, Kukura P, Mathies RA, Garavelli M, Cerullo G (2010) Conical intersection dynamics of the primary photoisomerization event in vision. *Nature* 467(7314):U440–U488
 38. Huntress MM, Gozem S, Malley KR, Jailaubekov AE, Vasileiou C, Vengris M, Geiger JH, Borhan B, Schapiro I, Larsen DS, Olivucci M (2013) Toward an understanding of the retinal chromophore in rhodopsin mimics. *J Phys Chem B* 117(35):10053–10070
 39. Segarra-Martí J, Garavelli M, Aquilante F (2015) Multiconfigurational second-order perturbation theory with frozen natural orbitals extended to the treatment of photochemical problems. *J Chem Theory Comput* 11(8):3772–3784
 40. González-Ramírez I, Segarra-Martí J, Serrano-Andrés L, Merchan M, Rubio M, Roca-Sanjuán D (2012) On the N1–H and N3–H bond dissociation in uracil by low energy electrons: a CASSCF/CASPT2 study. *J Chem Theory Comput* 8(8):2769–2776